Available online at www.sciencedirect.com
ScienceDirect
Journal of Power Sources 173 (2007) 437–449
JOURNAL OF POWER SOURCES
www.elsevier.com/locate/jpowsour

Fuel ejector design and simulation model for anodic recirculation SOFC system

Yinhai Zhu [a,b], Wenjian Cai [a,*], Changyun Wen [a], Yanzhong Li [b]

[a] School of Electrical and Electronic Engineering, Nanyang Technological University, Singapore 639798, Singapore
[b] School of Energy and Power Engineering, Xi'an Jiaotong University, Xi'an 710049, PR China

Received 3 July 2007; received in revised form 10 August 2007; accepted 13 August 2007
Available online 19 August 2007

Abstract

In this paper, a new modeling technique for fuel ejectors with high entrainment ratio, low pressure increment and over heated working gases in an anodic recirculation solid oxide fuel cell (SOFC) system is presented. By utilizing the thermodynamic, fluid dynamic principles and chemical constraints inside ejectors and employing a two-dimensional function to compute fluid velocity, the developed model involves no more than nine algebraic equations and this is very simple compared to all existing models. The detailed procedures for fuel ejector design and simulation are provided and its effectiveness is verified through simulation and compared with testing results. It shows that the proposed model is more accurate than presently available models, and therefore can be better used for ejector design and performance simulations. The ejector performances for both situations of stand-alone and integrated into the SOFC system are also studied.

Keywords: SOFC; Anodic recirculation; Ejector; Modeling; Design; Simulation

1. Introduction

Solid oxide fuel cell (SOFC) provides an effective means to convert chemical energy directly to electrical energy with high efficiency, flexible fuel utilization and very low pollutions [1–4], and this has drawn intensive research interests in recent years. A typical SOFC system includes a fuel cell stack and peripheral components such as fuel processor, heat exchanger, mixer and reformer. In the reformer, it is critical to have enough steam to prevent carbon deposition and provide sufficient heat for endothermic reforming reactions [5,6]. Since anodic exhausts are rich in steam and high in temperature, they can be recycled for fuel reforming by fans, blowers or ejectors. With no moving parts and less maintenance by using high pressure fuel gas as the primary fluid to suck the anodic exhausts, anodic recirculation using ejectors increases the SOFC system reliability compared with other schemes [7,8]. Since the cost of energy for fuel compression accounts for as high as 7% of the total cost of electricity [9], an extreme care should be taken in ejector design and operation for optimal system performance. Therefore, an accurate fuel ejector model for ejector design and the evaluation of on-design and off-design performances is essential.

The behaviors of an ejector related to entrainment capacity, steam to carbon ratio (STCR) and outlet temperature are strongly influenced by the geometries and operational conditions of the ejector. The performances of ejectors have been studied for decades and several modeling methods are available for ejectors design and performance evaluations [10–12]. However, most of the existing models are developed based on one-dimensional (1D) techniques for cooling and refrigeration applications. These modeling methods will cause large errors to model fuel ejectors in SOFC systems due to the differences in geometries, working fluids properties and operating conditions. Compared with traditional ejectors, fuel ejectors in an SOFC system are different mainly in the following aspects:

- The diameter ratio of mixing chamber to nozzle throat is much bigger [11], due to the requirement of larger entrainment ratio.
- The primary and secondary flows are overheated gases instead of saturated vapors.

* Corresponding author. Tel.: +65 6790 6862; fax: +65 6793 3318.
E-mail address: ewjcai@ntu.edu.sg (W. Cai).

0378-7753/$ – see front matter © 2007 Elsevier B.V. All rights reserved.
doi:10.1016/j.jpowsour.2007.08.036

Nomenclature

A	area (m^2)
C_p	specific heat of gas at constant pressure ($J\,kg^{-1}\,K^{-1}$)
D	diameter (m)
FC	fuel cell
k	specific heat ratio of gas
m	mass flow rate ($kg\,s^{-1}$)
M	Mach number
Mo	molecular weight ($kg\,mol^{-1}$)
n	molar flow rate ($mol\,s^{-1}$)
n_v	exponent in Eq. (12)
P	pressure (Pa)
r, R	radius (m)
R_g	gas constant ($J\,kg^{-1}\,K^{-1}$)
R_u	universal gas constant ($J\,mol^{-1}\,K^{-1}$)
T	temperature (K)
v, V	velocity ($m\,s^{-1}$)

Greek symbols

Ψ_P	isentropic coefficient of primary flow
ρ	density ($kg\,m^{-3}$)
ω	entrainment ratio, m_S/m_P
ξ_{exp}	coefficient accounting for friction loss during the mixing process

Subscripts

P	primary flow (i.e. high pressure fuel)
S	secondary flow (i.e. low pressure anodic recycle gas)
t	nozzle throat
0	ejector inlet
1	primary flow at nozzle throat
2	nozzle exit
3	mixing chamber inlet
4	diffuser exit

Superscripts

i	chemical component

- The secondary flow temperature is very high around 900 °C.
- The pressure increment of the secondary flow is much smaller.

To the best of the authors' knowledge, there are very few ejector models available for anodic recirculation SOFC systems. Marsano et al. developed an SOFC ejector model using 1D modeling technique for the evaluation of on-design and off-design performances [13]. Later, Ferrari et al. [14] improved the technique by dividing the ejector into serials of calculation cells where the governing equations are numerically solved. However, this model was also based on the 1D method. These 1D models assume that the velocity, pressure and temperature are uniformly distributed in the radial direction of the ejector. Based on this assumption 1D models can predict the performances of ejectors in traditional applications such as refrigeration within ±15% [11]. However, since the flow area of the secondary flow in an anodic recirculation ejector is much greater than that of traditional application ejectors, the conventional 1D modeling techniques will cause larger errors when applied in modeling SOFC ejectors.

In this paper, a simple yet accurate fuel ejector model for geometries design and performance evaluation is developed. The governing equations are derived through: (1) determining the primary mass flow rate by isentropic flow relations; (2) approximating the velocity distribution of secondary flow by a 2D function; (3) deriving a simple formula for secondary mass flow rate which is capable of dealing with the viscosity flow near the ejector inner wall and (4) establishing the energy conservation equation for the primary and secondary flows. The procedures for calculating ejector outputs are straightforward with no more than nine algebraic equations to be solved for both ejector design and performance simulation. To validate the effectiveness of the modeling technique for design, and performance evaluations at both on-design and off-design conditions, experimental numerical test and simulation studies have been carried out. Furthermore, the effects of pressure and temperature of primary flow and secondary flow, and chemical composition to the ejector performance on flow rate of anodic recycle gas, STCR, pressure, temperature and chemical composition at ejector outlet have also been studied. Finally, the performance of the fuel ejector in the SOFC system is investigated by varying the fuel inlet pressure, fuel cell pressure and fuel utilization. This model is expected to have wide applications in geometry design and performance evaluation of ejectors in anodic recirculation SOFC systems.

2. Anodic recirculation SOFC system with fuel ejector

A simplified sketch of a tubular SOFC is shown in Fig. 1 . It mainly consists of three components: an ejector, a reformer and a fuel cell stack.

The working principle of the tubular SOFC can be briefly descried as follows:

1. High pressure fuel (primary flow) passes through an ejector, where the low pressure anodic exhaust (secondary flow) is entrained and mixes with the primary flow. The resulting

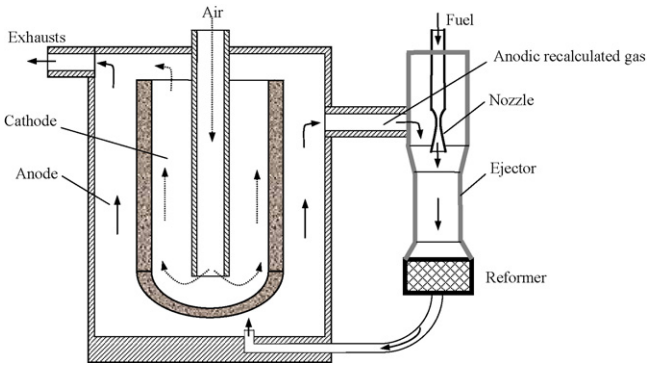

Fig. 1. Simplified sketch of a SOFC module.

mixing stream will shock in the diffuser to a higher pressure and then enter into the connected reformer. According to ref. [13], the function of the ejector is to re-circulate the anodic gas to

- raise the secondary flow pressure to meet the FC pressure at the required level;
- supply sufficient heat required for the reforming reactions in the reformer;
- provide sufficient secondary flow rate to maintain a proper STCR to avoid carbon deposition in the reformer and FC stacks.

2. Inside the reformer, highly endothermic reactions take place:

$$\text{Reforming}: \quad CH_4 + H_2O \leftrightarrow CO + 3H_2 \tag{1a}$$

$$\text{Shifting}: \quad CO + H_2O \leftrightarrow CO_2 + H_2 \tag{1b}$$

In the anodic recirculation SOFC system, the steam used for converting methane (or natural gas) into hydrogen in the reformer is supplied by the ejector. The required energy for reactions is provided by the sensible heat of the entrained high temperature secondary flow.

3. The reformed fuel is fed to the anode side of FC stack, while air is supplied to the cathode side. In the cathode, oxygen ions passing through the electrolyte layer react with hydrogen diffusing through the anode to form steam, and the electrons are released. These electrons pass through the external circuit and reach the cathode electrolyte layer, and thus the current flows though the closed circuit. The reactions inside the FC stack can be summarized as follows:

$$\text{Reforming}: \quad CH_4 + H_2O \leftrightarrow CO + 3H_2 \tag{2a}$$

$$\text{Shifting}: \quad CO + H_2O \leftrightarrow CO_2 + H_2 \tag{2b}$$

$$\text{Electrochemical}: \quad H_2 + 1/2\,O_2 \rightarrow H_2O \tag{2c}$$

In the anodic recirculation SOFC system, STCR, defined as

$$\text{STCR} = \frac{n_{H_2O}}{n_{CO} + n_{CH_4}} \tag{3}$$

is a very important parameter to evaluate carbon deposition in the reformer and FC stack. In terms of ejectors, the STCR can be evaluated by the entrainment ratio ω, defined as [10]

$$\omega = \frac{m_S}{m_P} \tag{4}$$

The entrainment ratio mainly depends on the ejector's geometries and the operation conditions such as the primary flow pressure, secondary flow pressure and the back pressure (reformer pressure). For a given ejector, the behavior of entrainment ratio is strongly influenced by the back pressure. As shown in Fig. 2 [11,15], there are three different operational modes for different back pressure: the critical mode, the sub-critical mode and the back flow mode. The maximum entrainment ratio is reached in the critical mode and is independent of the back pressure. As the back pressure increases from its critical value, the entrainment ratio drops rapidly, and then becomes zero or negative which implies that the ejector works at the back flow mode. From Fig. 2, it can also be seen that the entrainment ratio rises as the primary flow pressure decreases. Since an ejector should normally work at the critical mode, ejector performance only at the critical mode operation will be discussed in this work.

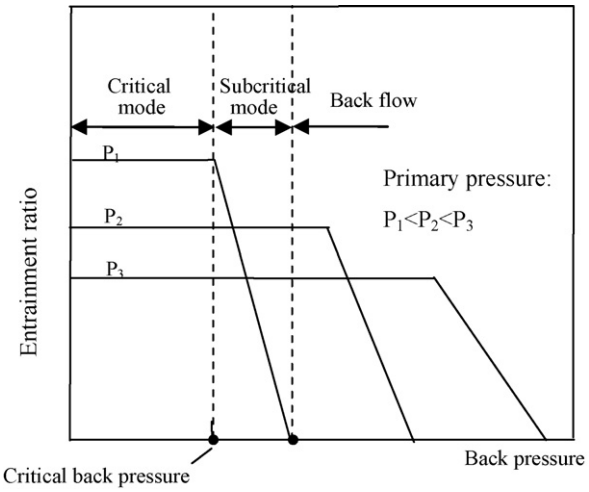

Fig. 2. Operational modes of ejector.

3. Governing equations

A schematic view of the flow characteristic and pressure distribution along the flow direction in a typical critical mode working ejector are shown in Fig. 3 . The value of pressure is indicated by the degree of color i.e. deeper color represents larger pressure. The primary flow shocks at the converging–diverging nozzle throat (Section 1) and discharges from the nozzle exit supersonically, while its pressure is substantially dropped. The primary flow then expands after the nozzle exit introduces a series of oblique shocks in the suction chamber and accelerates the entrained secondary flow to choking condition at Section 3. The secondary flow mixes with the primary flow after shocking in the mixing chamber. The mixed flow will shock at the end of

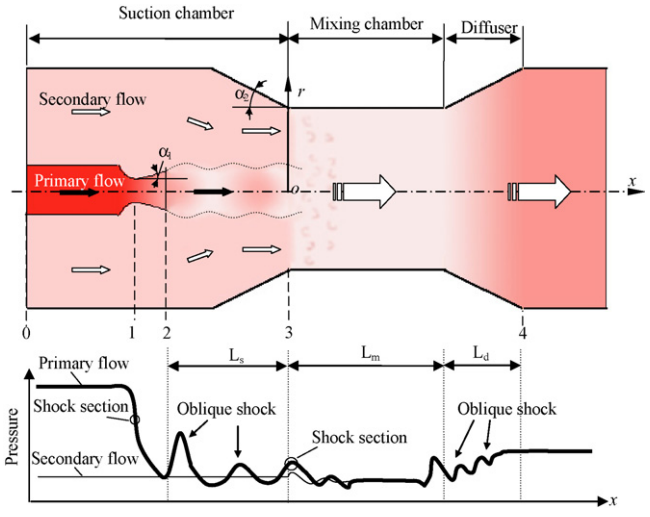

Fig. 3. Schematic diagram showing the flow characteristic and pressure distribution in ejector.

the mixing chamber and in the diffuser to convert kinetic energy into pressure to reach a higher value than that of the secondary flow inlet one [16,17].

Without loss of generality, the following assumptions are made in developing an ejector model for SOFC operation:

1. The velocity of the secondary flow inside the ejector is non-uniformly distributed in the radial direction and there exists velocity boundary layer near the inner walls of the ejector.
2. The primary flow velocity is uniform in the radial direction, as there is no boundary layer and that the flow area of the primary flow is much smaller than that of the secondary flow.
3. The primary flow is fully heated to the temperature of the secondary flow and the lost heat energy of secondary flow is negligible (i.e. $T_{S,3} = T_{S,0}$; $T_{P,3} = T_{S,0}$), since the amount of the secondary flow is generally about five times that of the primary flow and the temperature of the secondary flow is much higher than that of the primary flow.
4. Both the primary and the secondary flows are ideal gas inside adiabatic ejector walls.
5. Pressure and temperature of both the primary and the secondary flows are uniformly distributed inside ejector.
6. The isentropic relations hold in calculating friction losses.

3.1. Primary flow

Using the relations between velocity and Mach number at each section

$$V_{P,i} = M_{P,1}\sqrt{kR_g T_{P,i}}, \quad i = 1, 2, 3 \tag{5}$$

and the fundamental equation for ideal gas

$$C_p = \frac{kR_g}{k-1}, \tag{6}$$

the governing equations for the primary flow in the converging–diverging nozzle and the suction chamber are given as follows:

- Relations between Section 0 and Section 1

  Using the isentropic flow laws and energy balance, and taking the flow friction loss into consideration by multiplying an isentropic coefficient Ψ_P, we obtain the formula for the primary mass flow rate

$$m_{P,1} = \sqrt{\psi_P k R_g}\left(\frac{2}{k+1}\right)^{(k+1)/(2(k-1))} \rho_{P,0} A_t \sqrt{T_{P,0}} \tag{7}$$

  where the average gas constant and density of the fuel are defined as

$$R_g = \frac{R_u \sum_i n^i_{S,0}}{\sum_i n^i_{S,0} \mathrm{Mo}^i} \tag{8a}$$

  and

$$\rho_{P,0} = \frac{P_{P,0}}{R_g T_{P,0}} = \frac{P_{P,0}}{T_{P,0}} \frac{\sum_i n^i_{P,0} \mathrm{Mo}^i}{R_u \sum_i n^i_{P,0}} \tag{8b}$$

  for a mixture inlet fuel, respectively. The detailed derivation is given in Appendix A.

- Relations between Section 1 and Section 3

  Assuming that the primary flow fully expands after the nozzle exit into the suction chamber, and using the isentropic flow and energy balance laws for the primary flow from Section 1 to Section 3, we can obtain:

$$M_{P,3} = \sqrt{\frac{2(P_{P,0}/P_{S,0})^{(k-1)/k} - 2}{k-1}} \tag{9}$$

  and

$$V_{P,3} = M_{P,3}\sqrt{kR_g T_{S,0}} \tag{10}$$

- Diameter of primary flow at Section 3

To determine the flow area of the primary flow in Section 3, the mass and energy balance for the primary flow from Section 1 to Section 3 is required. The actual expansion diameter of primary flow at Section 3, $D_{P,3}$, is expressed by

$$D_{P,3} = \frac{D_t}{\zeta_{exp}}\sqrt{\frac{1}{M_{P,3}}}\left(\frac{2 + (k-1)M^2_{P,3}}{k+1}\right)^{(k+1)/(4(k-1))} \tag{11}$$

where ξ_{exp} is a coefficient accounting for the frictional loss due to the mixing of two flows. The details of deriving Eqs. (9) and (11) are presented in Appendix B.

3.2. Secondary flow

According to geometry features of a fuel ejector, flow area of the secondary flow is much greater than that of the primary flow. Due to the turbulence and viscosity of fluid, the velocities inside the ejector are non-uniformly distributed and there exists a velocity boundary layer in the secondary flow near the inner walls of the ejector as shown in Fig. 4 . In the traditional 1D model, both velocities of the primary flow and secondary flow are treated as constant in the radial direction. It is clear that this modeling method will cause large errors in modeling of fuel ejectors.

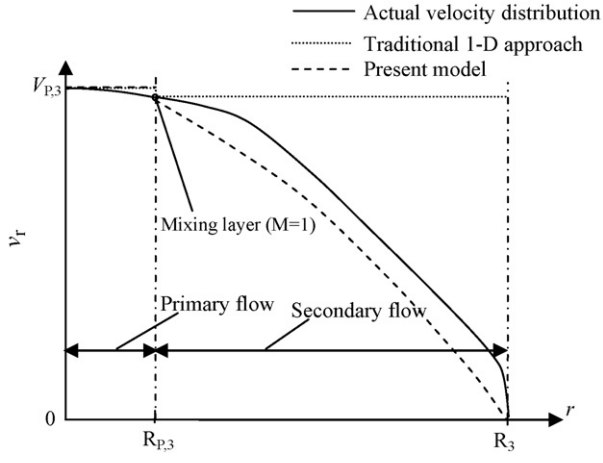

Fig. 4. Velocity distribution at the Section 3.

We now find out a simple yet accurate function to approximate the actual velocities inside the ejector. Considering that the function should satisfy (1) boundary conditions: $r=0$; $v_r = V_{P,3}$ and $r=R_3$; $v_r = 0$; (2) velocity characteristics of turbulent flow inside a pipe, we propose the following governing equation for the velocities of primary flow and secondary flow in Section 3

$$v_r = \begin{cases} V_{P,3} & 0 \le r \le R_{P,3} \\ V_{P,3}\left(\dfrac{R_3 - r}{R_3}\right)^{1/n_v} & R_{P,3} < r \le R_3 \end{cases} \tag{12}$$

where n_v is an exponent to be determined as follows.

At critical mode, it can be reasonably assumed that only the layer between the primary flow and secondary flow is in the choking condition ($M=1$) and the layer is very thin [12]. Therefore, from assumption 3, the velocity and the radius of the mixing layer are $v_r = \sqrt{kR_gT_{S,0}}$ and $r = R_{P,3} = D_{P,3}/2$, respectively. Substituting these values and Eq. (10) into Eq. (12), we obtain

$$n_v = \frac{\ln(1 - R_{P,3}/R_3)}{-\ln M_{P,3}} \tag{13}$$

The graph of v_r versus r is given as the dashed curve in Fig. 4. Clearly, it is quite close to the actual velocity distribution.

Based on this 2D expressional velocity of the secondary flow, we define the mean mass flow rate of secondary flow at Section 3 as

$$m_{S,3} = \int_{R_{P,3}}^{R_3} \bar{\rho} v_r \, dA \tag{14}$$

where $\bar{\rho}$ stands for the average density of secondary flow. Substituting Eq. (12) into Eq. (14) leads to the following integral equation:

$$m_{S,3} = 2\pi V_{P,3}\bar{\rho} \int_{R_{P,3}}^{R_3} \left(1 - \frac{r}{R_3}\right)^{1/n_v} r \, dr \tag{15}$$

By evaluating the integral of Eq. (15), the mass flow rate of the secondary flow can finally be expressed as

$$m_{S,3} = 2\pi V_{P,3}\bar{\rho} \left[\frac{n_v {R_3}^2}{n_v + 1}\left(1 - \frac{R_{P,3}}{R_3}\right)^{(n_v+1)/n_v} - \frac{n_v R_3^2}{2n_v + 1}\left(1 - \frac{R_{P,3}}{R_3}\right)^{(2n_v+1)/n_v} \right] \tag{16}$$

where the average density of the secondary flow is given as

$$\bar{\rho} = \frac{P_{S,0}}{R_g T_{S,0}} = \frac{P_{S,0}}{T_{S,0}} \frac{\sum_i n^i_{S,0}}{R_u \sum_i n^i_{S,0}} \tag{17}$$

3.3. Energy balance

For an ideal gas, the energy balance of the primary and secondary flow in the ejector can be described by

$$\sum_i m^i_{P,0} C^i_p T_{P,0} + \sum_i m^i_{S,0} C^i_p T_{S,0} = \sum_i m^i_4 C^i_p T_4 + E_{loss} \tag{18}$$

where the energy loss, E_{loss}, of primary flow and secondary flow in the ejector can be approximated as:

$$E_{loss} = \tfrac{1}{2}(1 - \xi_{exp}) m_{P,0} V^2_{P,3} \tag{19}$$

Remark. With this modeling method, the velocity of the major portion of the gas inside the fuel ejector, secondary flow, is accurately modeled by a 2D function. Because of this improvement, the modeling of complicated mixing process in the mixing chamber and diffusing in the diffuser is avoided in the present model. Note that the characteristics of the mixing process in the ejector have not been well understood yet. Therefore, the present model will result in less uncertainties or errors in the modeling of fuel ejectors in the SOFC system. Of course, this will simplify computation significantly. For example, for fuel ejector geometries design the model only consists of seven algebraic equations: Eqs. (3), (7), (9)–(11), (13) and (16).

4. Design and simulation procedures

4.1. Design procedure

The whole ejector design procedure is given as follows:

1. Specify the operating conditions, including:
   - fuel inlet mass flow rate m_P;
   - pressure and temperature of fuel inlet $P_{P,0}$ and $T_{P,0}$;
   - pressure and temperature of anodic recycle gas $P_{S,0}$; $T_{S,0}$;
   - chemical composition of fuel and anodic recycle gas;
   - STCR.
2. Determine the mass flow rate of anodic recycle gas m_S from Eq. (3).
3. Determine the nozzle throat area A_t from Eq. (7).
4. Compute the velocity of primary flow at mixing chamber inlet $V_{P,3}$ from Eq. (10)
5. Compute the diameter of active flow area of primary flow at mixing chamber inlet $D_{P,3}$ from Eq. (11).
6. Determine the radius of mixing chamber R_3 from Eqs. (13) and (16).

   The remaining steps are to follow the standard procedures in the design manuals [11,18], which are listed below for the completeness of the paper.
7. The angle employed in the divergent nozzle, α_1, ranges from 4° to 7.5°, with 5° to 6° most common.
8. The distance of nozzle exit to mixing chamber inlet, L_s, is around $1.5D_3$ for best performance. The angle of suction chamber, α_2, ranges from 3.5° to 5°.
9. The mixing chamber is typically $3D_3$ to $5D_3$ long to accommodate the shock pattern.
10. The diffuser is always conical in shape with an included angle range of 5–12° and 8–10° is most common. Its length, L_d, is usually $4D_3$ to $12D_3$ in practice.

A detail flowchart of the design procedure is shown in Fig. 5.

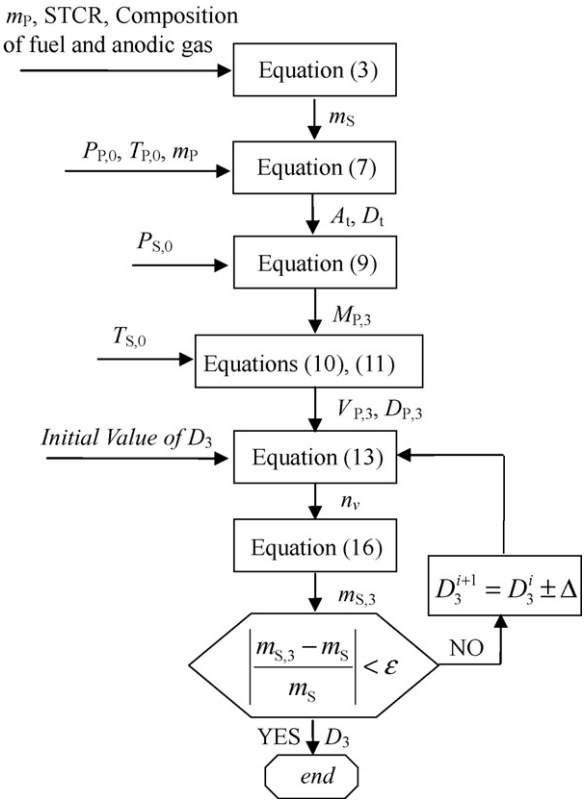

Fig. 5. Calculation flowchart for fuel ejector geometries design.

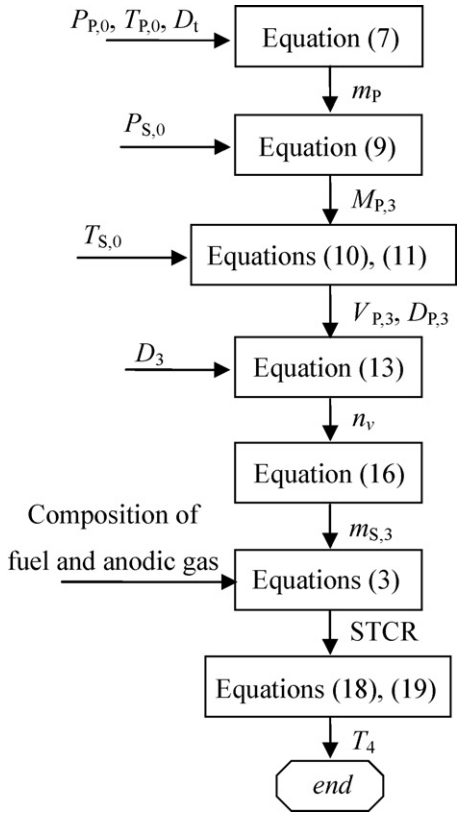

Fig. 6. Calculation flowchart for fuel ejector simulation.

4.2. Performance simulation procedure

For a given ejector geometry, its performance depends on the pressure $P_{P,0}$ and $P_{S,0}$, temperature $T_{P,0}$ and $T_{S,0}$, chemical composition of inlet fuel and anodic recycle gas, respectively. Since the main functions of the ejector in SOFC system are to meet the STCR at appropriate level and provide sufficient heat energy for the reforming reaction, the outputs at ejector exit are the entrainment ratio, STCR, temperature and chemical compositions. The procedure for performance simulation of the fuel ejector is very simple without iterative computation, which is given in the flowchart shown in Fig. 6.

5. Model comparisons and validation

The proposed models for ejector design and performance simulation will be validated from three aspects: design model validation, performance validation at on-design condition and performance validation at off-design conditions.

5.1. Design model validation

Table 1 shows typical values for an SOFC system [13]. Pure methane is used as fuel; the chemical compositions of the anodic exhaust are CH_4, H_2O, CO_2, CO and H_2. Two coefficients, Ψ_P and ξ_{exp}, used in the design are both taken as 0.98.

Starting with these data, the main parameters are obtained by following the proposed ejector design procedures as listed in Table 2 , in which the design data obtained by Marsano et al. [13] are also listed for comparison. It is shown from the table that the two critical ejector parameters: nozzle throat diameter and mixing chamber diameter agree fairly well. Even though the values of other parameters D_4, L_s, L_m and L_d are different, they are not critical since

1. given the same nozzle throat diameter and mixing chamber diameter, different design references gives different design parameters;
2. different values of D_4, L_s, L_m and L_d will not seriously affect on the ejector performance.

Table 1
Design point values of ejector

Parameter	Value
Fuel inlet	
Composition (molar, %)	CH_4 (100)
Flow rate (kg s^{-1})	0.0094
Pressure (bar)	10.06
Temperature (K)	673
Anodic recirculation gas	
Composition (molar, %)	H_2 (4.895) CO (3.785) H_2O (61.74) CO_2 (29.58)
Pressure (bar)	3.8
Temperature (K)	1280
Steam to carbon ratio	2.4

Table 2
Ejector design results

Parameter	Present model	Marsano et al. [13]
By calculation		
Nozzle, D_t (mm)	3.31	3.31
Mixing chamber, D_3 (mm)	19.98	20.04
By reference book		
D_4 (mm)	53.5	100.8
L_s (mm)	40.0	–
L_m (mm)	100.0	219.0
L_d (mm)	239.8	459.5

5.2. Performance validation at on-design condition

For comparison purpose, ejector geometries and inputs for both the proposed and the Marsano et al.'s model are taken from Marsano et al.'s ejector [13]. The main results obtained for the ejector on-design operation conditions are listed in Table 3. It is observed that the primary mass flow rate, secondary mass flow rate, entrainment ratio and STCR for both models agree very well, where the maximum difference is only 1.94%.

In the above two cases, the main advantage of the proposed model over Marsano's is the reduction of computational cost. As stated in Section 3, only modeling the flow inside the suction chamber of ejector is required by the present model, while modeling of the other two chambers such as mixing chamber and diffuser is not needed. In contrast to the present model, traditional 1D models need to apply the mass, energy and momentum conservation equations into each chamber to calculate the ejector performance.

5.3. Performance validation at off-design condition

Since the SOFC system load is usually adjusted through the fuel inlet flow rate, performance validation at off-design condition can be established by varying the fuel inlet pressure. The general performance of a refrigeration ejector obtained by experiment [15] and computational fluid dynamics (CFD) simulations [16] is shown in Fig. 7 , where the primary mass flow rate m_P rises linearly with the primary flow pressure in all the three operating modes. In contrast, the behavior of secondary flow is more complex.

- At low primary flow pressure, no secondary flow is entrained into the ejector.

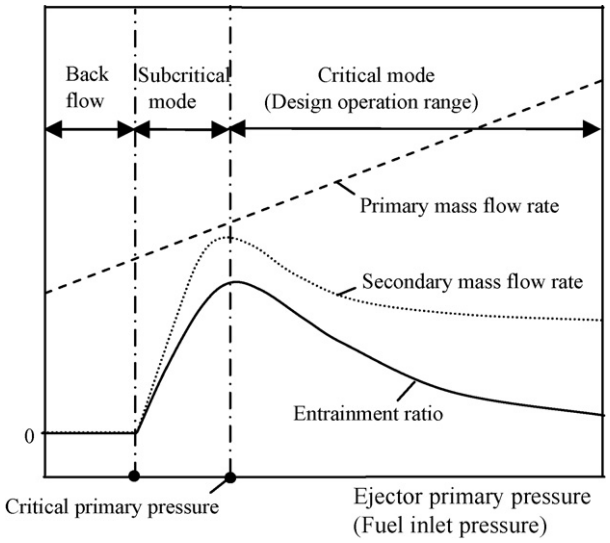

Fig. 7. Ejector performance at different primary pressures.

- As the primary flow pressure increases to the sub-critical region, the secondary flow is entrained proportionally and very sensible to the primary flow pressure. A maximum of secondary flow rate occurs when working conditions reaches the critical mode.
- In the critical mode, the secondary flow rate decreases and then remains quite constantly in the high primary flow pressure regions.

Since an ejector should normally work at the critical mode, ejector performance only at the critical mode operation will be discussed in the squeal.

Due to lack of experimental data, the validation will only be carried out through comparing the results of the proposed model with the experimental data obtained with Freon as the working fluid, where the mass flow rate and entrainment ratio versus the primary flow pressure are shown in Fig. 7. Although the working fluid of the experimental data is not methane, it can still be treated as ideal gas such that the basic assumptions for the model are still valid. Therefore, the trends of the mass flow rate and entrainment ratio versus the primary flow pressure obtained from the fuel ejector are the same as that in Fig. 7.

Keeping the fuel inlet (primary flow) temperature and anodic exhaust (secondary flow) conditions constant, the detail relationships between the two mass flow rates, entrainment ratio ω and the fuel inlet pressure are shown in Fig. 8 . The mass flow rate of the primary flow increases linearly with the fuel inlet pressure in accordance with Eq. (7), while the secondary mass flow rate and also the slope of the curve decrease gradually. In the

Table 3
Ejector simulation results

Parameter	Present model	Marsano et al. [13]	Δ = (Present's − Marsano's)/Marsano's
Primary mass flow rate, m_P (kg s^{-1})	0.0094	0.0094	0
Secondary mass flow rate, m_S (kg s^{-1})	0.0689	0.0677	0.0177
Entrainment ratio, ω	7.34	7.20	0.0194
STCR	2.44	2.40	0.0167

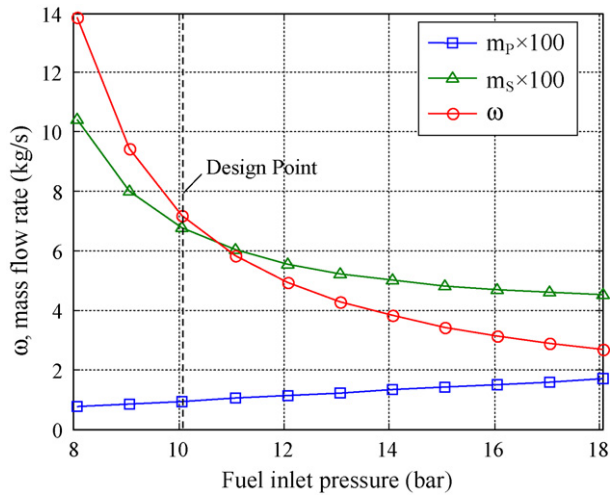

Fig. 8. Entrainment ratio and mass flow rate at different fuel inlet pressures.

high primary flow pressure region, the secondary mass flow rate is almost constant. These clearly agree with the critical mode experimental data shown in Fig. 7 well.

However, in Fig. 6 of ref. [13], both the secondary mass flow rate and entrainment ratio increase with increasing the primary flow pressure. Compared this to the experimental results, it is shown that the calculation error in Marsano's ejector model enlarges as the primary flow pressure increases. Inaccuracy of the 1D model is much larger when applying it in off-design ejector performance evaluation than in on-design performance evaluation, mainly because the velocity distribution varies a lot in the off-design conditions. The 1D model suffers from the assumption of the uniform velocity distribution which makes it generate large error in the fuel ejector performance evaluation at off-design conditions.

To explain in depth the phenomenon taking place inside the ejector, the relations of flow diameter $D_{P,3}$ and velocity $V_{P,3}$ of the primary flow at the cross Section 3 against the primary flow pressure are mapped in Fig. 9 . It shows that both the primary flow area and velocity increase as primary flow pressure increases. Consequently, the primary mass flow rate increases (Fig. 8). By noting that the diameter of mixing chamber is fixed, the flow area for the secondary flow is decreased while $D_{P,3}$ increases. Since the velocity of secondary flow is almost constant at critical working conditions, the secondary mass flow rate will decrease when primary flow pressure increases (Fig. 8).

6. Performance influence of other parameters

The ejector's performance is also affected by temperature of primary flow and secondary flow, pressure of secondary flow and chemical composition. In this section, we will study the effects of these parameters on the ejector performance on flow rate of anodic recycle gas, STCR, pressure, temperature and chemical composition at ejector outlet.

6.1. Influence of temperature

Fig. 10 shows that the behavior of two mass flow rates and entrainment ratio at different fuel inlet temperature. It is observed that the primary mass flow rate decreases for increased primary temperature, while the primary temperature does not influence on the secondary mass flow rate. This is in line with ESDU [19] that the temperature of super heated primary flow does not affect the secondary mass flow rate.

The relations between mass flow rates and secondary flow temperature are shown in Fig. 11 . It is seen that the secondary mass flow rate decreases as its temperature increases. This can be explained as follows: (1) higher temperature means lower density for a fixed pressure gas, resulting in less entrained secondary mass flow; (2) gas dynamic viscosity increases when temperature increases and pressure is constant. According to fluid dynamics principles, it is known that mass flow rate is reciprocal to the dynamic viscosity in turbulent flow.

6.2. Influence of secondary flow pressure

The relations between mass flow rate and secondary flow pressure are shown in Fig. 12 , where the secondary flow

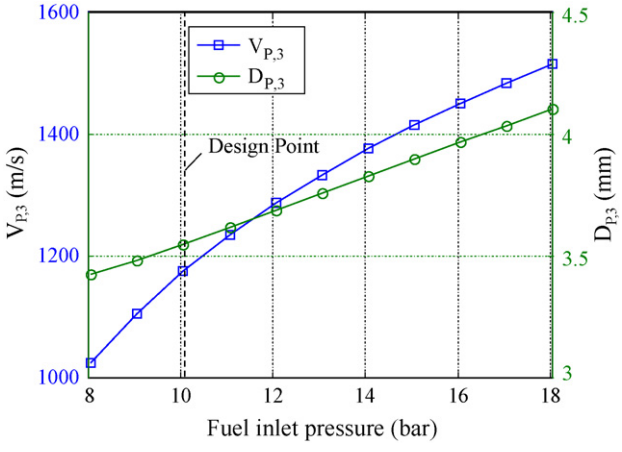

Fig. 9. Primary fluid velocity and flow diameter at Section 3 in different fuel inlet pressures.

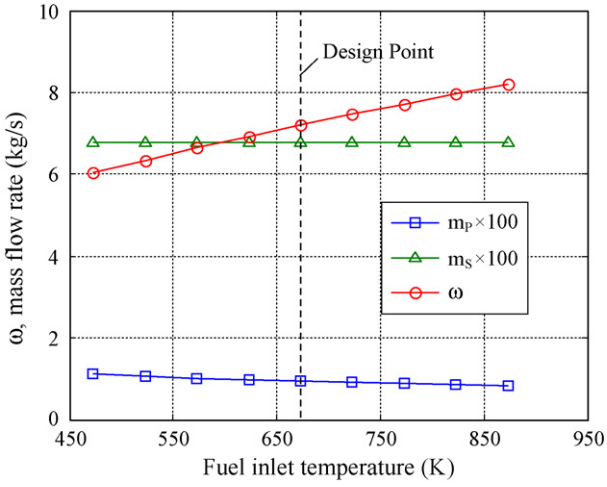

Fig. 10. Entrainment ratio and mass flow rate at different fuel inlet temperatures.

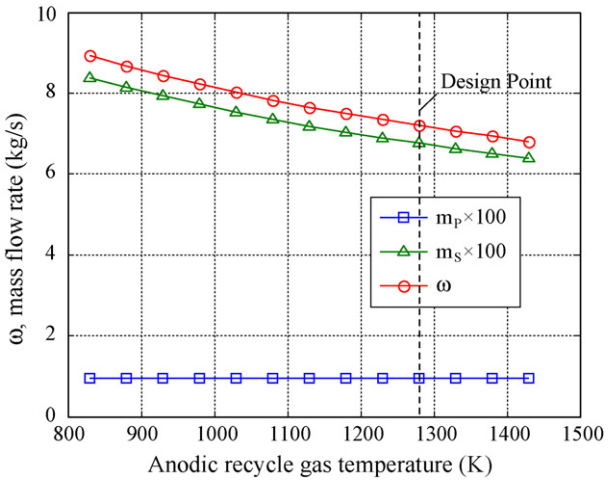

Fig. 11. Entrainment ratio and mass flow rate at different secondary temperatures.

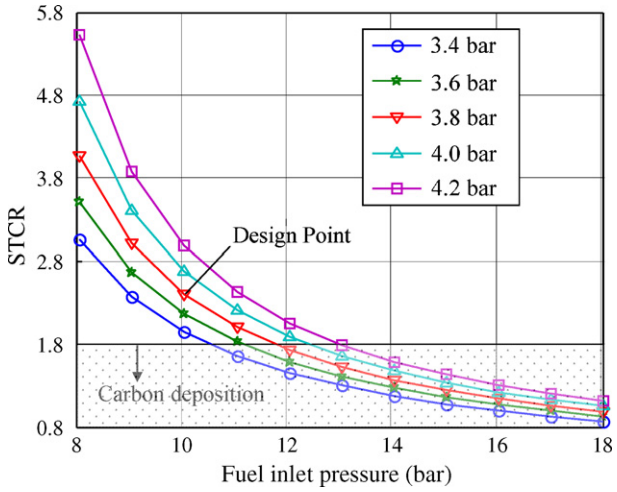

Fig. 13. STCR vs. fuel inlet pressure at different secondary pressures.

pressure has a strong influence on the secondary mass flow rate, as its density increases along with pressure when temperature is constant. Note that the fuel ejector is always working at its critical range (Fig. 7), i.e. the ejector exit pressure is always $1.015P_{S,0}$ when varying the secondary flow pressure.

Fig. 13 shows the influence of both primary flow pressure and secondary flow pressure on the ejector performance. The STCR decreases as the primary flow pressure increases, but increases with the increasing secondary flow pressure. For a designed value of the STCR between 1.8 and 2.4, it can easily drop below the limit if primary flow pressure is high, with an evident risk of carbon deposition.

Fig. 14 shows the influence of primary and secondary flow pressure on the ejector outlet temperature. The exit temperature decreases when primary flow pressure increases and secondary flow pressure decreases, as the temperature of primary flow is low while the secondary flow is high.

6.3. Influence of secondary flow chemical composition

The chemical composition of secondary flow depends on the fuel cell operating conditions. To analyze the effects of secondary flow composition on ejector performances and STCR, we define the molar rate of H_2O and CO_2 at anodic recycle gas, M_{HC}, as:

$$M_{HC} = \frac{n_{H_2O}}{n_{CO_2}} \tag{20}$$

while the other two chemical compositions, H_2 and CO, are constants of 4.895 and 3.785%, respectively. From Fig. 15 , it can be seen that the entrainment ratio ω decreases with increased M_{HC}, since the average density decreases as M_{HC} increases because the molecular weight of H_2O is lower than CO_2. The ratio STCR increases with the increasing M_{HC} but the slope of the curve decreases slightly and near constant at high M_{HC}, in line with the trends of entrainment ratio and secondary flow composition.

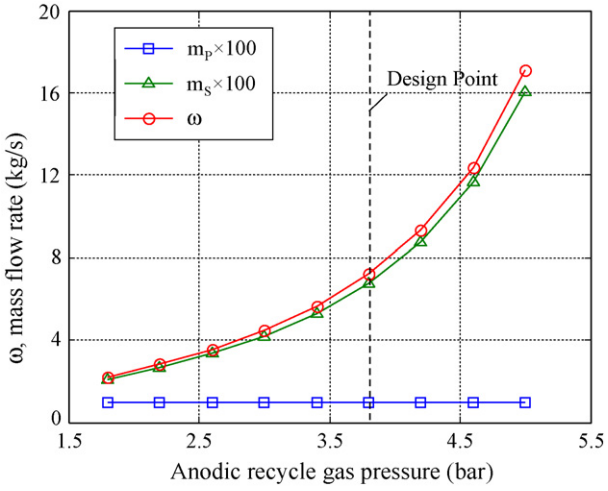

Fig. 12. Entrainment ratio and mass flow rate at different secondary pressures.

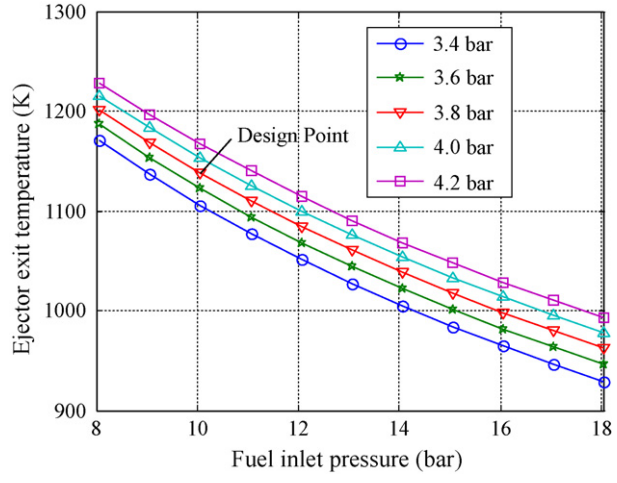

Fig. 14. Ejector exit temperature vs. fuel inlet pressure at different secondary pressures.

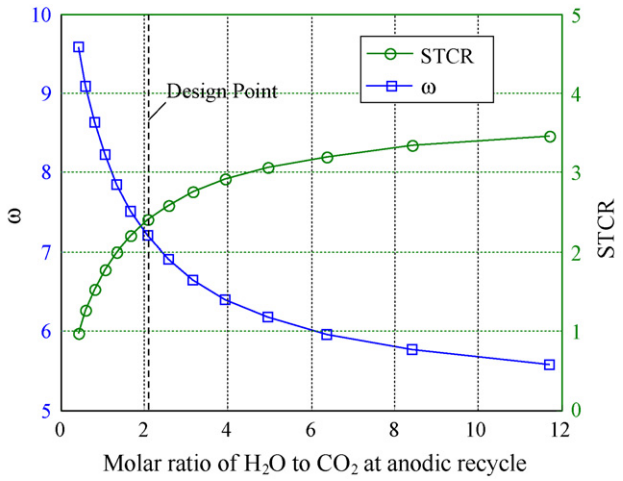

Fig. 15. ω and STCR in different chemical composition of secondary flow.

7. Effects on SOFC system performance

To study the influence of the fuel ejector on the anodic recirculation SOFC system, typical SOFC system design values are listed in Table 4 . Starting with these data, the main task is to predict the performance of the SOFC system (entrainment ratio, STCR, temperature at each components, cell voltage and cell power) on varying fuel inlet pressure, cell pressure and fuel utilization.

7.1. SOFC model

The SOFC model developed by [20] is adopted in this paper. The model allows the evaluation of the design and off-design behavior of the SOFC system under the influences of the cell operation pressure and temperature, the fuel and air utilizations, the current density, voltage, etc. During the calculations, the main assumptions are listed as follows:

1. Temperature within all the components of SOFC system is uniformly distributed.
2. Cathode flow is composed of 21% O_2 and 79% N_2. Fuel is pure CH_4.
3. The reforming and shifting reactions are at equilibrium in the reformer and FC stack.
4. Temperature of the gases at the outlet of the reformer and FC stack are equal to the reformer and FC stack temperature, respectively.
5. The pressure loss in FC stack is equal to 1.5% of the FC operation pressure.
6. The concentration loss is fixed at $1.5 \times 10^{-7}\ \Omega$.

Table 4
Design point values of SOFC

Parameter	Value
SOFC parameters	
Cathode thickness (cm)	0.035
Electrolyte thickness (cm)	0.017
Anode thickness (cm)	0.030
Overall cell area (m^2)	95
Operation conditions	
Fuel utilization	0.85
FC pressure (bar)	3.80
FC pressure loss (kPa)	5.7
Air inlet pressure (bar)	3.84
Air inlet temperature (K)	1000
Air flow rate (kg s^{-1})	0.47

In the simulation, we define the fuel utilization coefficient U_f as

$$U_f = \frac{n_{H_2}^{consumed}}{n_{H_2}^{in} + n_{CO}^{in} + 4n_{CH_4}^{in}} \quad (21)$$

where $n_{H_2}^{consumed}$ is the reaction rate of H_2 in the FC stack and $n_{H_2}^{in}$, n_{CO}^{in} and $n_{CH_4}^{in}$ are the molar flow rate of H_2, CO and CH_4 into the FC stack, respectively.

The simulation studies on the anodic recirculation SOFC system are carried out at different operation conditions by varying some key parameters, while keeping the cathode air pressure and temperature constant. The system consists of three model blocks: the fuel ejector, the reformer and the fuel cell stack. The parameters in the blocks are coupled and iterative computation is required:

- The inputs of fuel ejector are fuel inlet pressure and temperature, anodic recycle gas pressure, temperature and chemical composition; the outputs are ω, STCR, pressure, temperature and chemical composition at ejector exit.
- The temperature and chemical composition of the FC inlet gas are determined by reactions taking place in the reformer.
- In the FC stack, the values to be calculated are anode exhaust temperature, pressure, chemical composition, cathode exhaust temperature, chemical composition, FC voltage, current density, power, etc.

7.2. Ejector performance: integrated versus stand-alone

The ratios ω and STCR by varying the fuel inlet pressure are shown in Fig. 16 . They exhibit different behaviors but have sim-

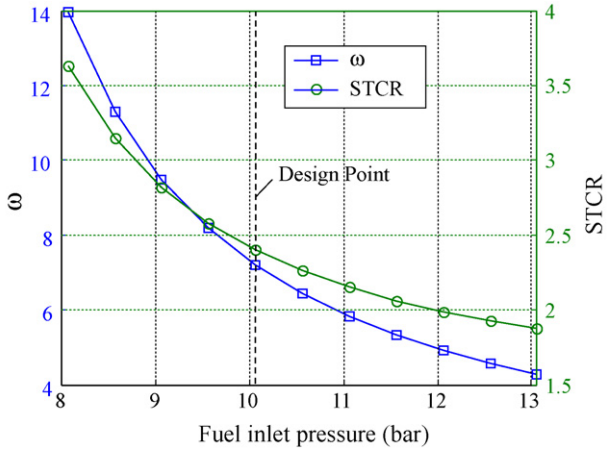

Fig. 16. ω and STCR at different primary pressures.

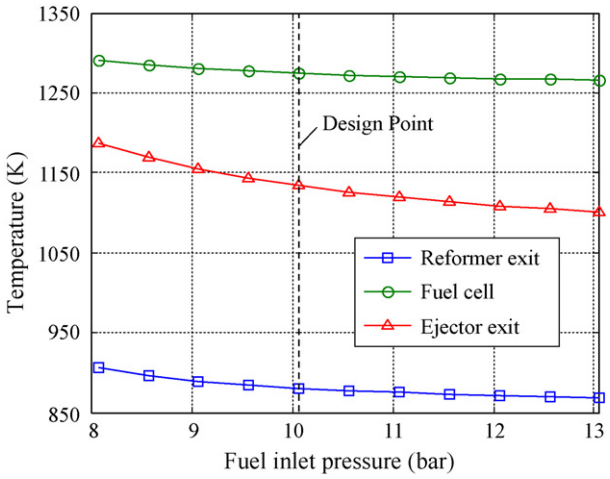

Fig. 17. SOFC system temperature at different primary pressures.

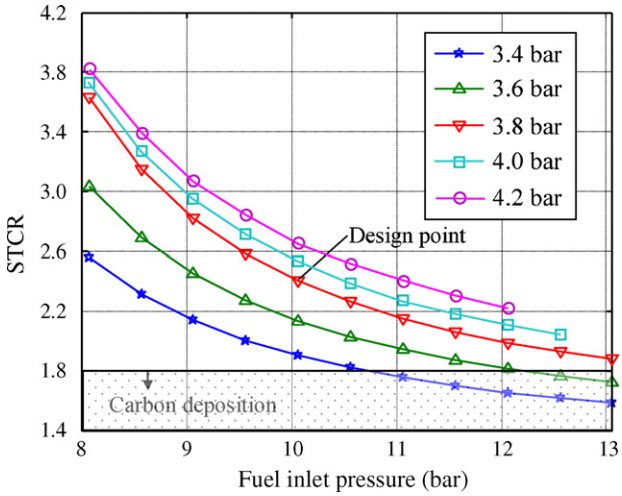

Fig. 19. STCR vs. primary pressure at different secondary pressures.

ilar trends with those obtained from Figs. 8 and 13, respectively. The differences are caused by that the temperature and chemical composition of the anodic recycle gas are always fixed at the design points in the stand-alone ejector, while they are affected by the FC stack when the ejector is used as a component in SOFC system. Compared with the ratio ω in Figs. 16 and 8, the maximum deviation is only 0.72% at $P_{P,0} = 8.06$ bar, which implies that the temperature and chemical composition of anodic recycle gas do not seriously affect the ejector entrainment ratio ω. However they have significant effect on STCR; the maximum deviation between integrated and stand-alone ejectors is 18.8%.

7.3. Components temperature

The gas temperature at each component for different fuel inlet pressure is shown in Fig. 17 . In all cases, the temperature decreases with increasing fuel inlet pressure, because of the primary flow is a low temperature fluid.

7.4. FC performance

The voltage, power and current density of fuel cell stack are obtained by varying fuel inlet pressure as shown in Fig. 18 . It is observed that the current density decreases with increasing fuel inlet pressure, which can be analyzed through the ejector off-design performance characteristic. On one hand, the flow rate of CH_4 into FC, $n^{in}_{CH_4}$, increases as the fuel inlet pressure increases as indicated in Fig. 8; On the other hand, the secondary flow rate significant decreases as fuel inlet pressure increases from Fig. 8, which decreases the flow rate of $n^{in}_{H_2}$ and n^{in}_{CO}. It is found that the reduction rate in $n^{in}_{H_2} + n^{in}_{CO}$ is higher than the increment rate in $4n^{in}_{CH_4}$ so that $n^{consumed}_{H_2}$ will finally decrease according to Eq. (21). This will cause the current density decreases as it is directly correlated with $n^{consumed}_{H_2}$. From Fig. 18, it is also seen that the FC voltage rises with the fuel inlet pressure as decreasing the FC stack temperature leads to a lower cell open circuit potential. The FC power increases with increasing the fuel inlet pressure and is almost constant at high fuel pressure.

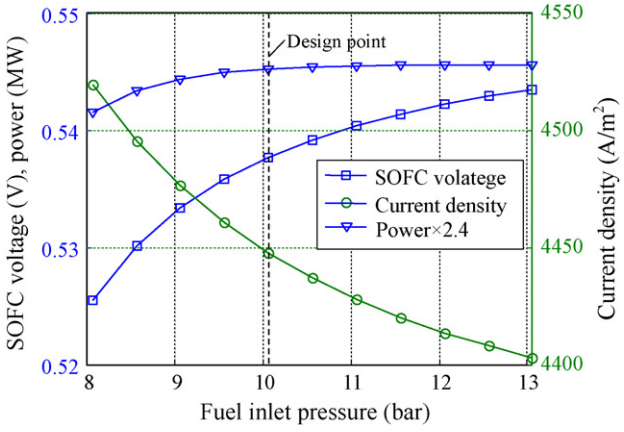

Fig. 18. SOFC voltage, current density and power at different primary pressures.

7.5. STCR

The STCR with the variation of the FC operation pressure is shown in Fig. 19 . It is quite different from that obtained in the

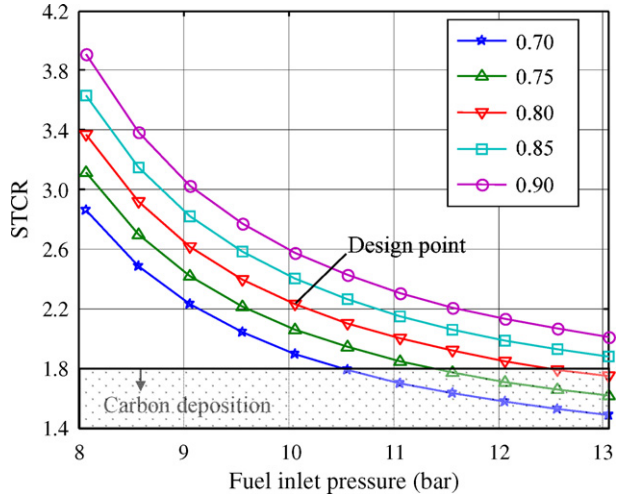

Fig. 20. STCR vs. primary pressure at different fuel utilizations.

stand-alone ejector (Fig. 13), especially in the ranges of low fuel inlet pressure and high FC pressure. This confirms that, for a FC pressure lower than 3.4 bar, the STCR can easily drop below the limited value and thus suffers from carbon deposition.

The results obtained by varying the fuel utilization factor at different fuel inlet pressures are shown in Fig. 20. This indicates that the STCR is strongly influenced by U_f. Note that U_f also has a direct effect on conversion rate of H_2 in FC stack, which affects the FC performances such as temperature, pressure and chemical composition at the anodic recycle gas. It shows that, for U_f lower than 0.7 the STCR can easily drop below the limited value.

8. Conclusions

In this paper, a new model for fuel ejector with large entrainment ratio, overheated working gas and low pressure increment in the anodic recirculation SOFC system is developed. The new model has no more than nine algebraic equations and can be applied in both ejector design and performance simulation. In contrast to the traditional 1D models, the new model has the following advantages:

1. The new model uses a 2D function to approximate the real velocity distribution inside the ejector. This makes it much more accurate than the traditional 1D model in describing the flow field inside the ejector (Fig. 4).
2. The modeling of flows in the mixing chamber and diffuser is not required by this model. In addition, throughout the modeling procedure, the energy conservation equation is not required for calculating the secondary mass flow rate. Both factors make present model simple and easy to apply.
3. It can be used for not only the on-design case but also off-design performance evaluations for ejectors in the anodic recirculation SOFC system, while the traditional 1D model is incapable for the off-design ejector performance prediction.

Furthermore, the ejector in the cases of on-design, off-design and integrated into an SOFC system performances have also been investigated. The main conclusions from the simulation results are summarized below:

1. Mass flow rate of the fuel increases with increased the fuel inlet pressure.
2. The behavior of STCR is similar to the secondary flow rate, which decreases as the fuel inlet pressure increases.
3. The temperature and chemical composition of anodic recycle gas do not seriously affect the ejector entrainment ratio ω, but have a significant impact on the ratio STCR.
4. The current density of SOFC stack decreases but its power output increases with increasing the fuel inlet pressure at constant fuel utilization.
5. The STCR can easily drop below the limited value causing the carbon deposition in high fuel inlet pressure regions.

The proposed model is expected to have wide applications in geometries design and performance evaluation of the ejectors in SOFC systems. Utilizing the model, our immediate future work will focus on validating the model effectiveness on performance evaluation at off-design operation conditions by experimental studies and investigating the influence of the cathode side and the fuel conditions on the performance of the fuel ejector and SOFC systems.

Appendix A. Primary flow relations between Section 0 and Section 1

Using the isentropic flow laws, the temperature and densities and pressures of primary flow at the Section 0 and Section 1, $T_{P,0}$, $T_{P,1}$, $\rho_{P,0}$, $\rho_{P,1}$, $P_{P,0}$, $P_{P,1}$, are related by

$$\frac{T_{P,1}}{T_{P,0}} = \left(\frac{\rho_{P,1}}{\rho_{P,0}}\right)^{k-1} \tag{A1}$$

and

$$\frac{T_{P,1}}{T_{P,0}} = \left(\frac{P_{P,1}}{P_{P,0}}\right)^{(k-1)/k} \tag{A2}$$

respectively.

Since the velocity at Section 0 is negligible compared with the velocity at Section 1, energy conservation equation of fuel from Section 0 to Section 1, and the mass flow rate at Section 1 are

$$C_p T_{P,0} = C_p T_{P,1} + \frac{V_{P,1}^2}{2} \tag{A3}$$

and

$$m_{P,1} = \rho_{P,1} A_t V_{P,1} \tag{A4}$$

respectively.

Considering the Mach number is 1 at Section 1, invoking Eqs. (5), (6) and (A3), we obtain

$$\frac{T_{P,0}}{T_{P,1}} = \frac{k+1}{2} \tag{A5}$$

Substituting Eq. (A5) into Eq. (5), results

$$V_{P,1} = \left(\frac{2kR_g T_{P,0}}{k+1}\right)^{1/2} \tag{A6}$$

Combining Eqs. (A1) and (A4)–(A6), and taking account the flow friction loss of an isentropic coefficient, Ψ_P, we finally obtain Eq. (7) for the primary flow mass flow rate.

Appendix B. Primary flow relations between Section 1 and Section 3

Since the primary flow expands fully in the suction chamber, ambient pressure of the expansion flow can be represented by the pressure of surrounding secondary flow $P_{S,0}$. Using the isentropic flow and energy balance laws for the primary flow from Section 1 to Section 3, we have:

$$\frac{T_{P,3}}{T_{P,1}} = \left(\frac{P_{S,0}}{P_{P,1}}\right)^{(k-1)/k} \tag{B1}$$

$$C_p T_{P,1} + \frac{V_{P,1}^2}{2} = C_p T_{P,3} + \frac{V_{P,3}^2}{2} \tag{B2}$$

where $T_{P,3}$ and $V_{P,3}$ are the temperature and velocity of primary flow at Section 3, respectively.

Multiplying Eq. (B1) by (A2), and adding Eq. (B2) to (A3), we obtain

$$\frac{T_{P,3}}{T_{P,0}} = \left(\frac{P_{S,0}}{P_{P,0}}\right)^{(k-1)/k} \tag{B3}$$

$$C_p T_{P,0} = C_p T_{P,3} + \frac{V_{P,3}^2}{2} \tag{B4}$$

Substituting Eqs. (5) and (6) into Eqs. (B3) and (B4) for Section 3, and using assumption 3, we obtain Eqs. (9) and (10).

To determine the flow area of the primary flow in the Section 3, the mass balances for the primary flow from Section 1 to Section 3 is required which can be expressed:

$$\rho_{P,1} A_t V_{P,1} = \rho_{P,3} A_{P,3} V_{P,3} \tag{B5}$$

using the isentropic flow laws, we obtain

$$\frac{\rho_{P,3}}{\rho_{P,1}} = \left(\frac{T_{P,3}}{T_{P,1}}\right)^{1/(k-1)} \tag{B6}$$

Substituting Eqs. (5) and (6) into Eq. (B2) for Sections 1 and 3, results

$$\frac{V_{P,3}}{V_{P,1}} = \frac{M_{P,3}\sqrt{kR_g T_{P,3}}}{\sqrt{kR_g T_{P,1}}} \tag{B7}$$

$$\frac{T_{P,1}}{T_{P,3}} = \frac{2 + (k-1)M_{P,3}^2}{2 + (k-1)} \tag{B8}$$

then substituted Eqs. (B6)–(B8) into Eq. (B5), the actual expansion diameter of primary flow at Section 3, $D_{P,3}$, corrected by a coefficient is obtained and expressed in Eq. (11).

References

[1] T.G. Benjamin, E.H. Camera, L.G. Marianowski, Handbook of Fuel Cell Performance, Institute of Gas Technology, 1995.
[2] Fuel Cell Handbook, sixth ed., U.S. Department of Energy, 2002.
[3] S.C. Singhal, K. Kendall, High Temperature Solid Oxide Fuel Cells, Elsevier, 2003.
[4] J. Larminie, A. Dicks, Fuel Cell System Explained, John Wiley and Sons Ltd., 2004.
[5] A.L. Dicks, J. Power Sources 61 (1996) 113–124.
[6] T. Takeguchi, Y. Kani, T. Yano, R. Kikuchi, K. Eguchi, K. Tsujimoto, Y. Uchida, A. Ueno, K. Omoshiki, M. Aizawa, J. Power Sources 112 (2002) 588–598.
[7] EG&G Services-Parson Inc., Science Application International Corporation, Fuel Cell Handbook, fifth ed., US DOE, 2000.
[8] J.H. Keenan, E.P. Neumann, F. Lustwerk, Proceedings of the Annual Meeting on ASME, 1949, pp. 299–309.
[9] R. Peters, E. Riensche, P. Cremer, J. Power Sources 86 (2000) 432–441.
[10] I.W. Eames, S. Aphornratana, H. Haider, Int. J. Refrig. 18 (1995) 378–386.
[11] B.J. Huang, J.M. Chang, C.P. Wang, V.A. Petrenko, Int. J. Refrig. 22 (1999) 354–364.
[12] Y. Zhu, W.J. Cai, C.Y. Wen, Y. Li, Energy Convers. Manage. 48 (2007) 2533–2541.
[13] F. Marsano, L. Magistri, A.F. Massardo, J. Power Sources 129 (2004) 216–228.
[14] M.L. Ferrari, A. Traverso, L. Magistri, A.F. Massardo, J. Power Sources 149 (2005) 22–32.
[15] D.-W. Sun, Energy Sources 19 (1997) 349–367.
[16] Y. Bartosiewicz, Z. Aidoun, P. Desevaux, Y. Mercadier, Int. J. Heat Fluid Fl. 26 (2005) 56–70.
[17] E. Rusly, L. Aye, W.W.S. Charters, A. Ooi, Int. J. Refrig. 28 (2005) 1092–1101.
[18] ASHRAE, Steam-jet Refrigeration Equipment, Equipment Handbook, ASHRAE, 1979.
[19] ESDU, Ejectors and Jet Pumps, Data Item 86030, ESDU International Ltd., London, 1985.
[20] P. Costamagna, L. Magistri, A.F. Massardo, J. Power Sources 96 (2001) 352–368.